Science and Technology of
Advanced Materials

Modular high-throughput test stand for versatile screening of thin-film materials libraries

To cite this article: Sigurd Thienhaus *et al* 2011 *Sci. Technol. Adv. Mater.* **12** 054206

IOP Publishing Science and Technology of Advanced Materials
Sci. Technol. Adv. Mater. **12** (2011) 054206 (7pp) doi:10.1088/1468-6996/12/5/054206

Modular high-throughput test stand for versatile screening of thin-film materials libraries

Sigurd Thienhaus, Sven Hamann and Alfred Ludwig

Institute for Materials, Ruhr-Universität Bochum, 44780 Bochum, Germany

E-mail: alfred.ludwig@rub.de

Received 20 June 2011
Accepted for publication 11 October 2011
Published 16 December 2011
Online at stacks.iop.org/STAM/12/054206

Abstract
Versatile high-throughput characterization tools are required for the development of new materials using combinatorial techniques. Here, we describe a modular, high-throughput test stand for the screening of thin-film materials libraries, which can carry out automated electrical, magnetic and magnetoresistance measurements in the temperature range of −40 to 300 °C. As a proof of concept, we measured the temperature-dependent resistance of Fe–Pd–Mn ferromagnetic shape-memory alloy materials libraries, revealing reversible martensitic transformations and the associated transformation temperatures. Magneto-optical screening measurements of a materials library identify ferromagnetic samples, whereas resistivity maps support the discovery of new phases. A distance sensor in the same setup allows stress measurements in materials libraries deposited on cantilever arrays. A combination of these methods offers a fast and reliable high-throughput characterization technology for searching for new materials. Using this approach, a composition region has been identified in the Fe–Pd–Mn system that combines ferromagnetism and martensitic transformation.

Keywords: combinatorial materials science, thin films, high-throughput characterization, ferromagnetic shape memory alloys, Fe–Pd–Mn, electrical measurements, magnetic measurements

1. Introduction

The combinatorial material synthesis approach allows us to produce, in a single experiment, thin film materials libraries that contain up to about 5000 samples on a single substrate. To efficiently identify new or optimized materials, screening methods, i.e. tools for automated materials characterization, must be designed and applied. The goal is to establish high-throughput measurement techniques capable of locating the regions of optimal properties in materials libraries.

In this paper, we present a custom-designed high-throughput test stand, which was applied to the screening of an Fe–Pd–Mn materials library, a system of interest for ferromagnetic shape memory alloys (FSMAs). Thin SMA films can be used as sensors [1] and actuators [2] in microelectromechanical systems owing to their one-way or two-way shape memory and superelasticity [3–5]. The reason for the shape memory effects lies in the thermoelastic, reversible martensitic transformation. Switching frequencies in conventional, i.e. non-ferromagnetic, SMA systems are limited to less than 100 Hz [6] owing to the slow thermal response of SMAs. In contrast, FSMAs exhibit the magnetic-field-induced strain (MFIS) effect where the reorientation of the domains is magnetically driven, allowing much higher actuation frequencies in the kHz range [7, 8].

Generally, SMA films are characterized by their thermal or stress hysteresis curves, from which transformation temperatures and the maximum achievable stress can be determined. They can be evaluated by, for example, the cantilever method [9] or differential scanning calorimetry (DSC) [10]. However, DSC has a low throughput, as it measures a single sample of a thick freestanding film

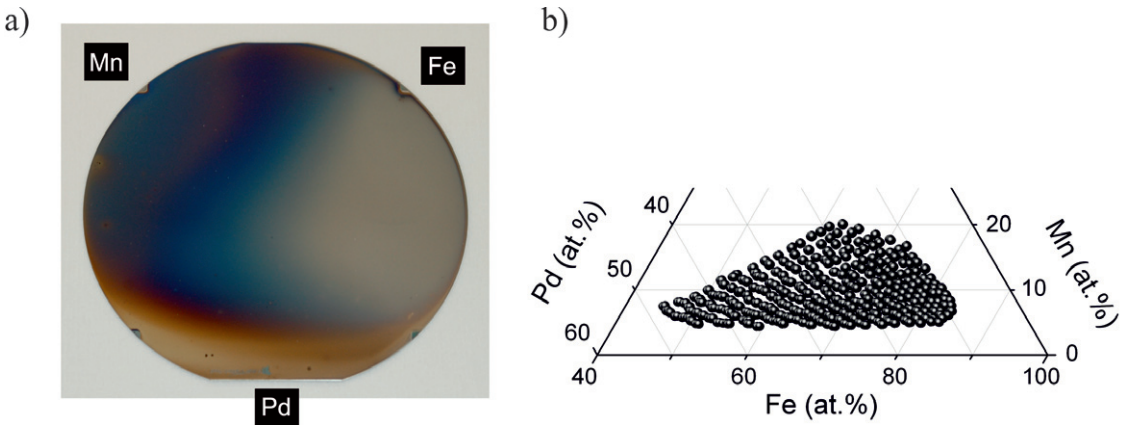

Figure 1. (a) Photograph of a continuous composition spread-type Fe–Pd–Mn materials library deposited and annealed on a 4 in Si/SiO_2 wafer and (b) partial ternary diagram showing the range of fabricated Fe–Pd–Mn compositions as measured by EDX.

at a time, and is not suitable for thin films with a low hysteresis [11]. Parallel inspection methods for measuring the shape memory actuator effect based on micromachined cantilever arrays have been reported [12]. Structural and magnetic phase transformations are accompanied by changes in electrical resistance [13–15]. Temperature-dependent resistance measurements ($R(T)$) have been used to characterize SMA thin films [16], allowing us to determine the transformation temperature and hysteresis width. A detailed magnetic analysis can be performed, for example, using a vibrating sample magnetometer; however, it requires delicate manual handling of individual samples and is therefore a low-throughput method. The magneto-optical Kerr effect (MOKE) allows adequate screening, which can be performed on the wafer level. Different approaches such as epitaxial growth of Fe–Pd films by sputtering [17], pulsed laser deposition [18] and e-beam evaporation [19] have been applied to fabricate FSMA thin films.

There is a need to substantially improve the properties of the binary Fe–Pd alloy by adding other elements. Certain prerequisites must be met for new FSMAs: they need to show a reversible martensitic transformation at temperatures above 25 °C; they should be ferromagnetic with a high Curie temperature, for example $T_C > 250$ °C; and they should contain a single phase. To exhibit the MFIS effect, a high magnetocrystalline anisotropy in the martensitic state and a high mobility of the martensitic twin boundaries are necessary. In this study, we used a modular high-throughput test stand to efficiently identify these intrinsic properties. This approach was previously used to characterize the intrinsic properties of the Fe–Pd–Cu system [20], and here, we applied it to the Fe–Pd–Mn system. The addition of Mn to Fe–Pd is of interest because of the following reasons: Mn suppresses the irreversible transformation from a face-centered tetragonal (fct) structure to a body-centered cubic (bcc) structure; it increases the martensitic transformation temperature [21] and can undergo an antiferromagnetic-to-ferromagnetic transformation when alloyed into Fe–Pd [22]. The results of this screening are used to identify the composition regions that are promising for a further detailed study of the MFIS effect.

2. Experimental details

2.1. Deposition of thin-film materials libraries

The Fe–Pd–Mn materials library discussed in this paper (figure 1(a)) was fabricated by simultaneous sputtering from three cathodes located in a circular geometry over the substrate (target–substrate distance; 185 mm). The tilted cathodes naturally result in a wedge-type thickness gradient across the sample. Elemental targets (diameter: 100 mm; purity: 99.99%) were used for the deposition.

The substrate was a 4-in-diameter Si wafer with a 1.5-μm-thick thermal SiO_2 diffusion barrier layer. The base pressure at the beginning of the deposition was $<5 \times 10^{-5}$ Pa. During the deposition, the pressure was adjusted to 0.665 Pa with an Ar (6N) flow rate of 60 $cm^3\,min^{-1}$. For a detailed description of the sputtering system, see [23]. After deposition, the materials library was annealed in a vacuum furnace (Schmetz, type IU 54 1F) at 850 °C for 0.5 h under a N_2 pressure of 80 kPa to prevent Mn loss by sublimation. The wafer was quenched from 850 °C to room temperature by N_2 overpressure (40 kPa) with a cooling rate of approximately 15 °C s^{-1} to prevent precipitate segregation. After deposition and subsequent annealing, the compositions at 301 points across the materials library were determined using automated energy dispersive x-ray spectroscopy (EDX; figure 1(b)) measurements in a scanning electron microscope (JSM 5800, Oxford X-Act detector). x-ray diffraction (XRD) measurements were carried out with an X'Pert PRO MPD system (Cu K_α radiation, spot size: ~3 mm, PIXcel detector) to reveal the crystal phases in the materials library after annealing.

2.2. Modular high-throughput test stand

For the screening of materials libraries, a versatile wafer mapping system has been constructed. Its different modules can be used for temperature-dependent electrical (resistance, figure 2(b)), magnetic (MOKE, figures 2(a) and (c)) and combined (magnetoresistance) measurements. During the measurements, the materials library is placed on a holder whose temperature is varied from −40 to 300 °C. With

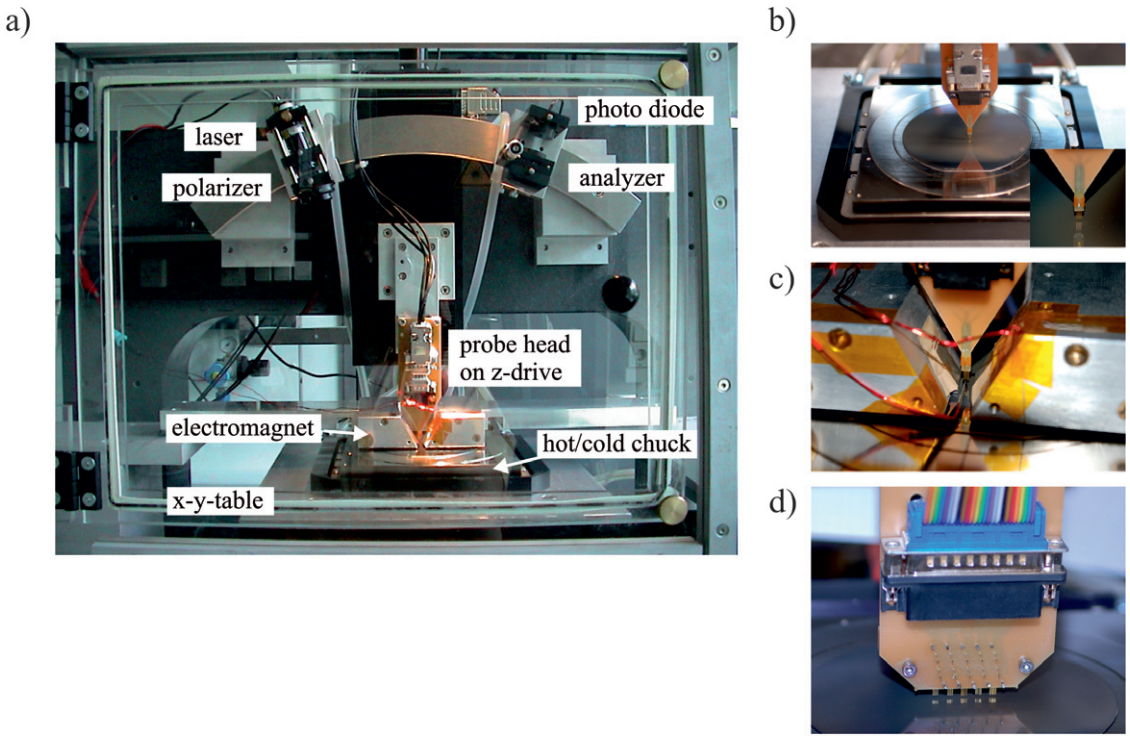

Figure 2. (a) Overview of the high-throughput test stand, with the MOKE setup and resistance probe head installed, (b) the sample holder with a 4 in wafer and a four-pin probe head for resistance measurements, (c) closer view of the magnet and probe head during magnetoresistance measurements and (d) special probe head with five groups of four spring-contact probes.

a special setup, temperature can be swept from −100 to 300 °C in the single-sample measurement mode. The sample size is variable up to 6-inch- diameter wafers. Samples are kept in place by suction through vacuum channels. The holder is mounted on an automated *x*–*y* table and can be positioned with μm accuracy. The apparatus is placed inside a flowbox purged with N_2 to prevent water condensation at low temperatures and oxidation at high temperatures. All measurement sequences are programmed using LabView software.

2.2.1. Resistance mapping and temperature-dependent resistance measurements. Resistance mapping is useful in overviewing the phases present, as resistance varies among different phases as well as between single- and multiple-phase regions. $R(T)$ measurements are used to identify phase transformations during temperature cycling, indicated by hysteresis in the $R(T)$ curve. Reversible changes in electrical resistance indicate structural transformations such as martensitic transformations [24].

Resistance measurements are carried out using custom-made four-point probe heads. The probe consists of four spring contacts (diameter <0.3 mm) with an equidistant spacing of about 0.5 mm. Its head is fixed on a computer-controlled vertical translation stage (*z*-stage), which is situated above the sample holder. Up to twenty contact probes can be used during each measurement: five groups of four pins (figure 2(d)) or 20 pins in a row. They are controlled using a switching matrix and a source meter (Keithley, models 707 and 2400).

For the resistance mapping of a materials library at room temperature, a probe head with four pins is used. The software controls the movement of the *x*–*y* table and the *z*-stage. The edge of the wafer or a characteristic feature on the wafer is taken as a positioning reference. Each spot is measured three times to improve statistics. Using a 2 mm step in the *x*- and *y*-directions results in the rapid accumulation of several thousands of resistance values. The $R(T)$ measurements can be carried out in two ways:

(a) *Wafer mapping mode*: the four-point probe measures predefined locations across the entire wafer, which is kept at a constant temperature, then the temperature is changed stepwise (e.g. in 5 °C steps) and the measurement is repeated. The mode is relatively fast: cycling up and down through a temperature interval from 0 to 150 °C in 5 °C steps takes around 32.5 h for 301 points (a typical materials library size), that is, 6.5 min per point. However, the data can be noisy because the position of the pins can be shifted due to thermal drift.

(b) *Single-sample mode*: the four-point probe is lowered onto the measurement point and the temperature is scanned. This type of measurement offers a higher signal-to-noise ratio, because the pins are not repositioned, but it takes a longer time. A special probe head with five four-contact probes was developed to speed up the procedure by measuring five samples in parallel. Nevertheless, the wafer mapping mode remains faster; it is used to overview the thin film library, and the single-sample mode is then applied for more detailed measurements of selected locations.

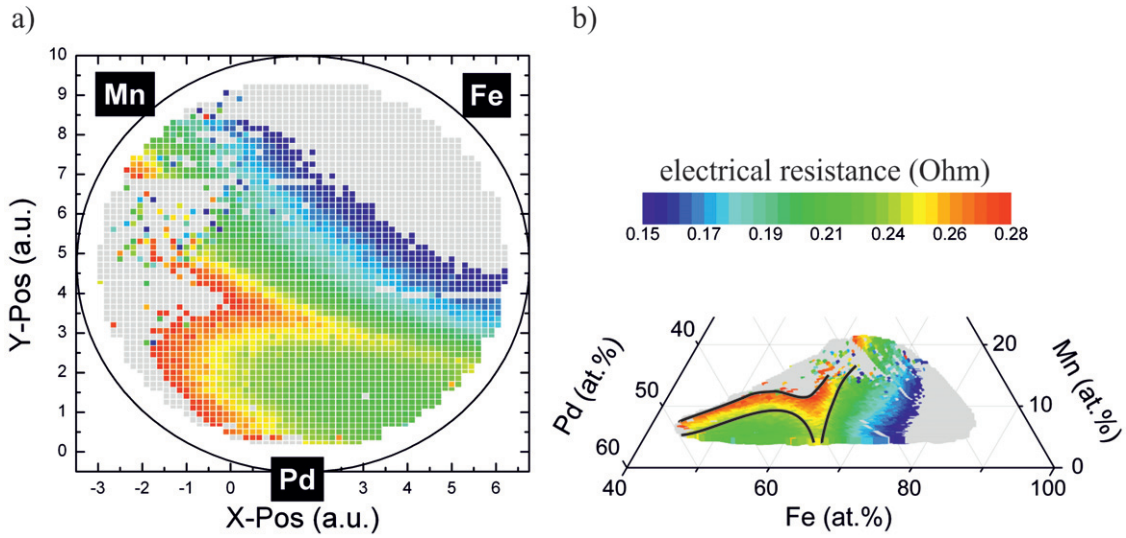

Figure 3. (a) A 3082-point resistance map of the Fe–Pd–Mn materials library and (b) section of a ternary composition diagram with color-coded resistance values, where lines are added for clarity.

2.2.2. Magnetic measurements. The main purpose of using this screening method is to identify samples showing ferromagnetism at room temperature, which is important for FSMAs. A custom-designed water-cooled electromagnet is installed, supplying a maximum magnetic flux density of about 0.3 T between its pole shoes. The magnet is attached to an adjustable frame; thus, the gap between the materials library and the pole shoes is kept constant at approximately 1 mm, giving sufficient space for moving the library underneath the magnet. A MOKE system consisting of a 5 mW multimode laser diode ($\lambda = 670$ nm), a polarizer, an analyzer and a photodiode is set up to measure the intensity of reflected light. A Hall sensor is positioned between the pole shoes to measure the magnetic field. The photodiode signal is read out using a lock-in amplifier to detect small changes in intensity. A special probe head is designed to fit in the gap between the pole shoes, thus enabling magnetoresistance measurements (resistance is measured while the magnetic field is cycled). Both MOKE and magnetoresistance measurements can be carried out as temperature-dependent screening measurements across the entire materials library.

2.2.3. Cantilever array measurements. Owing to its modular concept, the test stand can be further equipped with a position sensor (Micro-epsilon, optoNCDT 1401). This setup can be used to measure the change in curvature of cantilever arrays [25]. For screening measurements using this module, the laser must be focused at the end of a cantilever while the temperature is being cycled. Using the Stoney equation and the geometrical dimensions of the setup allows the calculation of changes in stress with temperature. For information on the fabrication of cantilever arrays, deposition of materials libraries on these structures and measurement of actuators with this setup, see [26, 27].

3. Results and discussion

3.1. Electrical characterization

Resistance mapping was performed across the materials library at room temperature. The step size was set to 1.5 mm in the *x*- and *y*-directions, resulting in 3082 measurement points. Each point was measured three times for better statistics. For clarity, only the regions of interest are colored in figure 3, while the areas with high or low resistances are gray. Electrical connection can deteriorate between the sample and the pins during the measurements. Therefore, these measurements were further excluded (colored in gray). Only 301 composition points were measured by EDX and thus the results were linearly interpolated on the 3082 spots of the resistance map. This interpolation is valid because of the close proximity of the measurement points. The resulting resistance-composition data were color-mapped in the ternary composition diagram (figure 3(b)).

$R(T)$ measurements were carried out to determine compositions that undergo a reversible phase transformation. The measurements were made in the wafer mapping mode in the temperature range of 0–150 °C in 5 °C steps. The results are presented in figure 4: although the $R(T)$ curves of samples without phase transformation are monotonic (figure 4(c)), a martensitic transformation is manifested by hysteresis (figure 4(d)). The $R(T)$ curves provide further details of the hysteresis parameters and transformation temperatures. The analysis is done manually and is therefore time-consuming. For a quick overview, the regions across the materials library were assigned numbers between 0 (non-transforming) and 1 (transforming) using the derivative of the smoothed $R(T)$ curve. All values were normalized by the difference between the maximum and minimum values.

3.2. Magnetic characterization

Using the MOKE setups, 301 points across the Fe–Pd–Mn materials library were measured at room temperature in

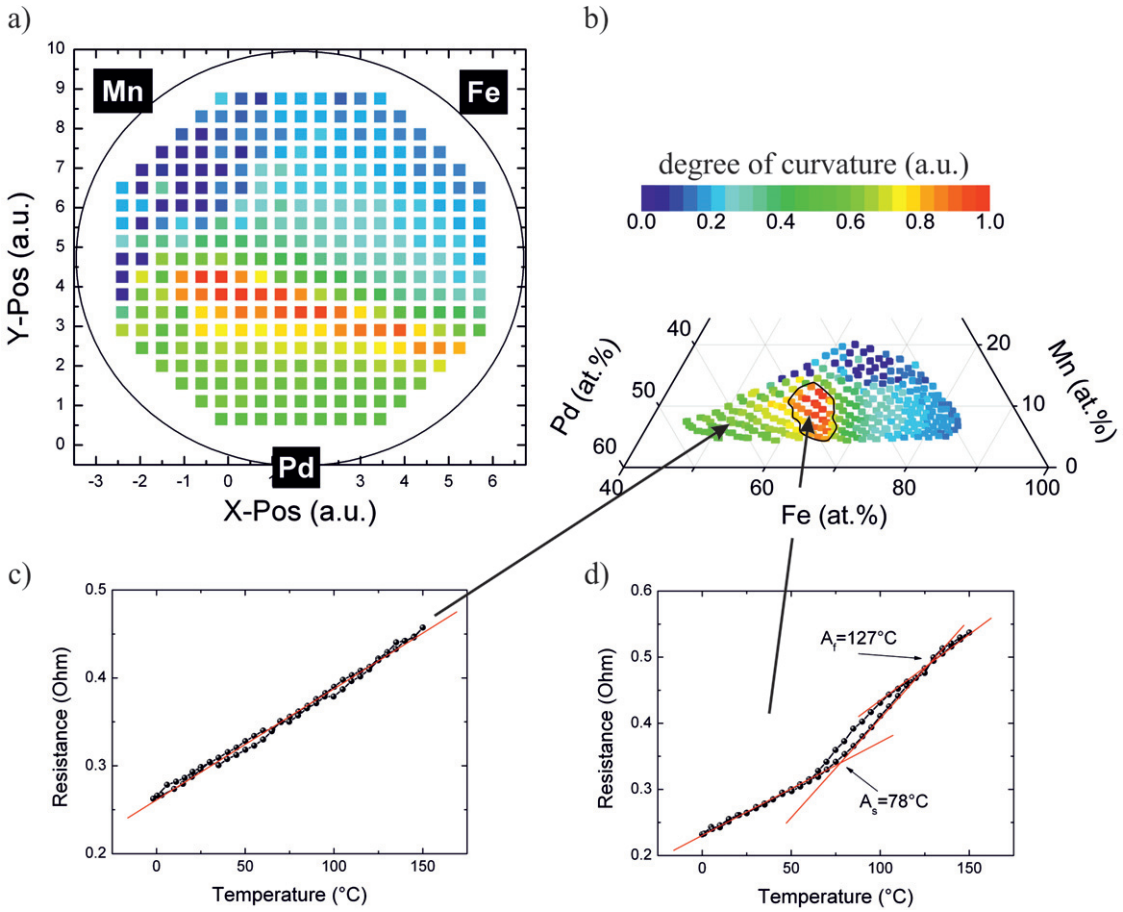

Figure 4. (a) $R(T)$ map of the Fe–Pd–Mn materials library. (b) $R(T)$ results shown in a section of the ternary composition diagram, where regions showing a martensitic transformation are enclosed by the black line. (c, d) Examples of $R(T)$ curves without ((c), $Fe_{51.1}Pd_{42.8}Mn_{6.1}$) and with ((d), $Fe_{68.5}Pd_{26.8}Mn_{4.7}$) a martensitic transformation.

4.5 mm steps. The electromagnet was cycled between −300 and +300 mT. While the data for non-ferromagnetic points are featureless (figure 5(c)), the magnetic sections of the materials library display hysteresis curves with sudden changes in MOKE intensity (figures 5(d) and (e)). To compare the resulting data, the curves were automatically assigned numbers between 0 (no hysteresis) and 1 (well-pronounced hysteresis) using the derivative of the MOKE curve. The derivative was normalized by a noise factor evaluated using the difference between the maximum and minimum values on the MOKE curve. Measurements of the magnetoresistance of the materials library (not shown) yielded values of $\Delta R/R \approx 0.1\%$ at a maximum magnetic flux of 300 mT.

3.3. Discussion

The screening of the magnetic properties of the Fe–Pd–Mn materials library using the MOKE revealed ferromagnetic and non-ferromagnetic regions in the composition diagram, as shown in figure 5. All samples are ferromagnetic on the Fe-rich side of the phase diagram (Fe > 80 at.%), while no ferromagnetic behavior is observed in the Fe-poor region (Fe <55 at.%) and in the region with Mn content above 12 at.%. The remaining area shows both ferromagnetic and nonferromagnetic sections depending on the Pd and Mn contents.

The $R(T)$ measurements revealed a region in the phase diagram where samples undergo a martensitic transformation, and these results were confirmed by temperature-dependent XRD analysis (results not shown). This region is also identified in the room-temperature resistance map through its elevated resistance. A comparison of the maps reveals a region exhibiting both magnetic and phase-transformation behavior, with contents of 60–66 at.% Fe, 6–8 at.% Mn and 28–32 at.% Pd. This result suggests that to produce Fe–Pd–Mn FSMAs, Mn must be added to the $Fe_{70}Pd_{30}$ system at the expense of Fe, keeping the Pd content approximately constant. XRD mapping (figure 6) revealed that this composition range corresponds to an fct phase, in good agreement with previously reported results [21, 22]. Although the solubility of Mn in Fe–Pd was reported as <2.5 at.% [21], it was found that Mn content up to 12 at.% can be dissolved at decreased Fe contents without any precipitation as determined by XRD. The region showing a single fct phase (encircled by a black line) is very narrow and lies within multi-phase areas. At lower Fe concentrations, an fcc structure, similar to the $Fe_{50}Pd_{50}$ phase, and Pd precipitates (red squares) appear. When the amount of Fe is increased to above 65 at.%, the Fe–Pd bcc phase (gray inverted triangles) develops with remaining fractions of the transforming fct phase. This result explains the observation of hysteresis in the $R(T)$ curves,

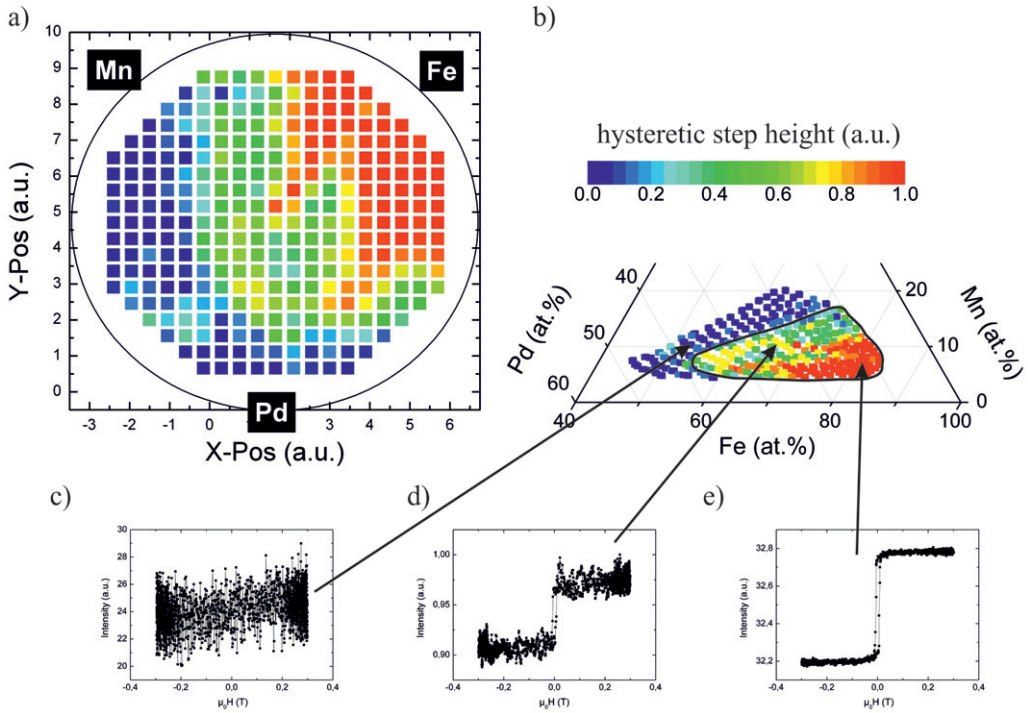

Figure 5. (a) A 301-point MOKE map of the Fe–Pd–Mn materials library; (b) The same results shown in a section of the ternary composition diagram, where the ferromagnetic region with well-defined hysteresis is enclosed by the black line. (c–e) MOKE curves of non-ferromagnetic ((c), $Fe_{63.2}Pd_{19.7}Mn_{17.1}$) and ferromagnetic ((d), $Fe_{72.4}Pd_{15.8}Mn_{11.8}$ and (e), $Fe_{82.1}Pd_{12.3}Mn_{5.6}$) samples.

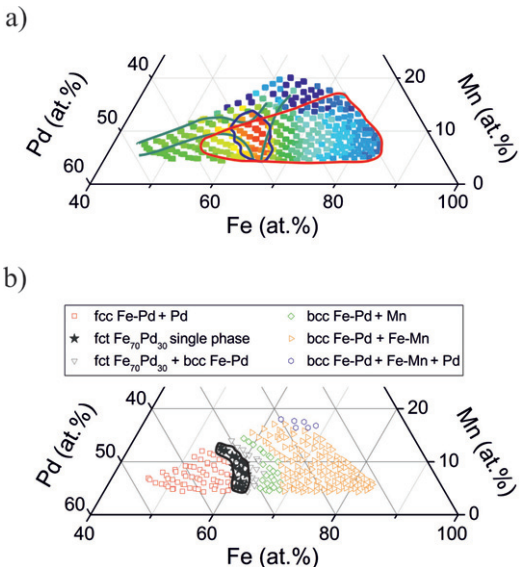

Figure 6. (a) Superposition of all measurement results in the Fe–Pd–Mn materials library defining a region of interest. (b) Overview of the different phases determined by XRD analysis. A comparison of (a) and (b) reveals a single fct-phase region, as determined by XRD analysis, which exhibits both a martensitic transformation and ferromagnetism. This region is enclosed by a black line in (b) and meets the prerequisites of the MFIS effect.

where a martensitic transformation only appeared within the fct grains of the films. Increasing the Fe content results in Mn and then Fe–Mn precipitation.

To clarify the phase formation and magnetic properties of the Fe–Pd–Mn system, further investigations are being carried out focusing on the identified concentration region.

Additional measurement techniques can be added to the described high-throughput measurement system, such as a force sensor or a digital holography system.

4. Conclusions

In this paper, the benefit of a versatile high-throughput test stand with a range of property measurement modules has been demonstrated by screening an Fe–Pd–Mn materials library for FSMA compositions. Various fully automated mapping methods, namely resistance at room temperature, temperature-dependent resistance and MOKE measurements, were applied. The characteristic changes in parameters allowed the identification of interesting compositions, such as those of FSMA alloys showing ferromagnetism and hysteresis-like nonlinearity of the $R(T)$ curves. These compositions were then studied by XRD analysis to determine their crystallographic phase. A very narrow single-phase area, as determined by XRD analysis, which accommodates up to 12 at.% of Mn without forming precipitates, was found. These results show the advantage of the high-throughput test stand in identifying new systems and screening different properties in a large number of samples.

Acknowledgments

We acknowledge support from Deutsche Forschungsgemeinschaft (DFG) within the priority programme SPP 1239 (S H) and the Heisenberg programme (A L). We thank Y W Lai for his help in optimizing the MOKE and A Savan for support.

References

[1] Bechtold C, Teliban I, Thede C, Chemnitz S and Quandt E 2010 *Sensors Actuators* **158** 224
[2] Zarnetta R, Ehmann M, Savan A and Ludwig A 2010 *Smart Mater. Struct.* **19** 065032
[3] Miyazaki S and Ishida A 1999 *Mater. Sci. Eng.* A **273–275** 106
[4] Gupta V, Martynov V and Johnson A D 2002 *Actuator* **2002** 355
[5] Winzek B, Schmitz S, Rumpf H, Sterzl T, Hassdorf R, Thienhaus S, Feydt J, Moske M and Quandt E 2004 *Mater. Sci. Eng.* A **378** 40
[6] Tomozawa M, Kim H Y and Miyazaki S 2009 *Acta Mater.* **2** 441
[7] Murray S J *et al* 1998 *J. Appl. Phys.* **83** 7297
[8] James R D and Wuttig M 1998 *Phil. Mag.* A **77** 1273
[9] Winzek B, Sterzl T, Rumpf H and Quandt E 2003 *J. Physique.* IV **112** 1163
[10] Rumpf H, Winzek B, Zamponi C, Siegert W, Neuking K and Quandt E 2004 *Mater. Sci. Eng.* A **378** 429
[11] Zarnetta R, König D, Zamponi C, Aghajani A, Frenzel J, Eggeler G and Ludwig A 2009 *Acta Mater.* **57** 4169
[12] Takeuchi I *et al* 2003 *Nat. Mater.* **2** 180
[13] Pollock D D 1985 *Electrical Conduction in Solids* (Metals Park, OH: American Society for Metals) p 148
[14] Bozorth R M 1951 *Ferromagnetism* (New York: Van Nostrand)
[15] Hamann S, Ehmann M, Thienhaus S, Savan A and Ludwig A 2008 *Sensors Actuators* A **147** 576
[16] Zarnetta R *et al* 2010 *Adv. Funct. Mater.* **20** 1917
[17] Bechtold C *et al* 2010 *Adv. Mater.* **22** 1
[18] Buschbeck J, Hamann S, Ludwig A, Holzapfel B, Schultz L and Faehler S 2010 *J. Appl. Phys.* **107** 113919
[19] Edler T, Hamann S, Ludwig A and Mayr S G 2011 *Scr. Mater.* **64** 89
[20] Hamann S *et al* 2010 *Acta Mater.* **58** 5949
[21] Sánchez-Alarcos V, Recarte V, Pérez-Landazábal J I, González M A and Rodríguez-Velamazán J A 2009 *Acta Mater.* **57** 4224
[22] Hamann S, Savan A, Thienhaus S and Ludwig A 2008 *Actuator 2008 Conf. Proc.*
[23] Ludwig A, Zarnetta R, Hamann S, Savan A and Thienhaus S 2008 *Int. J. Mater. Res.* **99** 1144
[24] Buschow K H J, Cahn R W, Flemming M C, Ilschner B, Kramer E J and Mahajan S 2001 *Encyclopedia of Materials: Science and Technology* 4152
[25] Ludwig A, Cao J, Savan A and Ehmann M 2007 *J. Alloys Compd.* **446–447** 516–21
[26] Ludwig A, Cao J, Brugger J and Takeuchi I 2005 *Meas. Sci. Technol.* **16** 111
[27] Vitushinsky R, Schmitz S, Winzek B and Ludwig A 2009 *J. Microelectromech. Syst.* **18** 186